Biomimetic divalent ligands for the acute disruption of synaptic AMPAR stabilization

ARTICLE *in* NATURE CHEMICAL BIOLOGY · FEBRUARY 2011

Impact Factor: 13 · DOI: 10.1038/nchembio.498 · Source: PubMed

9 AUTHORS, INCLUDING:

Matthieu Sainlos
French National Centre for Scientific Resea…
27 PUBLICATIONS **819** CITATIONS
SEE PROFILE

Cezar Tigaret
University of Bristol
16 PUBLICATIONS **355** CITATIONS
SEE PROFILE

Christel Poujol
Université Victor Segalen Bordeaux 2
40 PUBLICATIONS **830** CITATIONS
SEE PROFILE

Lucie Bard
University College London
11 PUBLICATIONS **307** CITATIONS
SEE PROFILE

nature chemical biology

ARTICLE

PUBLISHED ONLINE: 26 DECEMBER 2010 | DOI: 10.1038/NCHEMBIO.498

Biomimetic divalent ligands for the acute disruption of synaptic AMPAR stabilization

Matthieu Sainlos[1–3,5], Cezar Tigaret[2,3,5], Christel Poujol[3,4], Nelson B Olivier[1], Lucie Bard[2,3], Christelle Breillat[2,3], Kevin Thiolon[2,3], Daniel Choquet[2,3]* & Barbara Imperiali[1]*

The interactions of the AMPA receptor (AMPAR) auxiliary subunit Stargazin with PDZ domain–containing scaffold proteins such as PSD-95 are critical for the synaptic stabilization of AMPARs. To investigate these interactions, we have developed biomimetic competing ligands that are assembled from two Stargazin-derived PSD-95/DLG/ZO-1 (PDZ) domain–binding motifs using 'click' chemistry. Characterization of the ligands *in vitro* and in a cellular FRET-based model revealed an enhanced affinity for the multiple PDZ domains of PSD-95 compared to monovalent peptides. In cultured neurons, the divalent ligands competed with transmembrane AMPAR regulatory protein (TARP) for the intracellular membrane-associated guanylate kinase resulting in increased lateral diffusion and endocytosis of surface AMPARs, while showing strong inhibition of synaptic AMPAR currents. This provides evidence for a model in which the TARP-containing AMPARs are stabilized at the synapse by engaging in multivalent interactions. In light of the prevalence of PDZ domain clusters, these new biomimetic chemical tools could find broad application for acutely perturbing multivalent complexes.

The ionotropic glutamate receptor subfamily of AMPARs mediates most fast excitatory synaptic transmission in the mammalian central nervous system. Variation in the AMPAR type and population at the postsynaptic density (PSD) is a fundamental feature of synaptic plasticity, which is the essential basis for learning and memory[1]. The regulation of receptor populations results from a fine interplay between modulation of the surface expression, trafficking and stabilization of receptors at the synapse. AMPARs are heterotetrameric ligand-gated ion channels assembled from GluA1-GluA4 (GluR1-GluR4) pore-forming subunits that determine the biophysical properties of the channel and regulate their intracellular trafficking. In mammalian neurons, most AMPAR channels associate with nonconducting subunits from the TARP, cornichon homolog or CKAMP44 protein family members, which control both channel gating and trafficking[2]. We and others have previously shown that the interaction between the TARP Stargazin and the scaffold protein PSD-95 is essential to trapping and transiently stabilizing the diffusing AMPARs at the PSD[3,4]. This interaction directly involves the C-terminal residues of Stargazin and the PDZ domains of the postsynaptic membrane-associated guanylate kinases (MAGUKs) such as PSD-95. Furthermore, this stabilization process does not rely on other AMPAR complex PDZ domain–binding motifs, such as those from the cytosolic C-terminal tail of GluA2 (ref. 3). Currently, the molecular detail of the endogenous interactions and the roles that they play in the synaptic AMPAR population dynamics is poorly defined because of the dearth of methods for acutely and specifically controlling the binding interactions.

In this context, we sought to develop a chemically based approach for acutely disrupting endogenous AMPAR–TARP complex interactions with postsynaptic MAGUKs. The perturbation of specific protein-protein interactions by synthetic ligands that represent a sequence from one interaction partner is a standard approach. Indeed, minimal peptides derived from the C-terminal PDZ domain–binding motifs of various proteins have been used successfully to compete against interactions with the respective cognate PDZ domain–containing proteins[5–7]. However, this approach has not been reported for the AMPAR complex interaction with PSD-95, and initial attempts with short peptides derived from the C-terminal motif of Stargazin have failed to show evidence of perturbation at subtoxic concentrations. This observation contrasts with the strong effect on AMPAR function induced by PDZ domain–binding-deficient mutants of Stargazin *in vivo*[3,4] and suggests a distinct mode of stabilization for the AMPAR–Stargazin–PSD-95 interaction. Therefore, considering the supramolecular arrangement of the two ensembles of binding partners, we hypothesized that multivalency might play a significant role in stabilizing the AMPAR–TARP–MAGUK assemblies.

Multivalent binding is an important biological phenomenon that is broadly implemented in cells to regulate protein-protein and protein-ligand interactions in various contexts, including transcription factor–DNA, antigen-antibody, virus-cell and bacterial toxin–cell interactions[8]. The advantages of this mode of interaction result from an enhancement of selectivity and/or affinity and include discrimination between different protein oligomerization states and stabilization of functional protein complexes. The role of multivalency has not been addressed in the case of AMPAR complex stabilization at the synapse. Despite the complexity of the transient interactions formed by the TARP-containing AMPAR complex and the postsynaptic MAGUKs, three features emerge from consideration of the supramolecular assemblies that might promote multivalent interactions (**Fig. 1**). First, although the exact stoichiometry of TARP per AMPAR remains unclear, and may vary depending on cell type[9–12], recent models of hippocampal neurons suggest the presence of either two or four units per receptor[11]. Hence, synaptic TARP-containing AMPAR complexes would present two or more identical PDZ domain–binding motifs from the auxiliary subunits. Second, postsynaptic MAGUKs, which are key elements of the PSD architecture[13], share the same domain topology

[1]Department of Chemistry and Department of Biology, Massachusetts Institute of Technology, Cambridge, Massachusetts, USA. [2]Centre National de la Recherche Scientifique, Unité Mixte de Recherche 5091, Bordeaux, France. [3]Université de Bordeaux, Bordeaux, France. [4]Bordeaux Imaging Center, Bordeaux, France. [5]These authors contributed equally to this work. *e-mail: dchoquet@u-bordeaux2.fr or imper@mit.edu

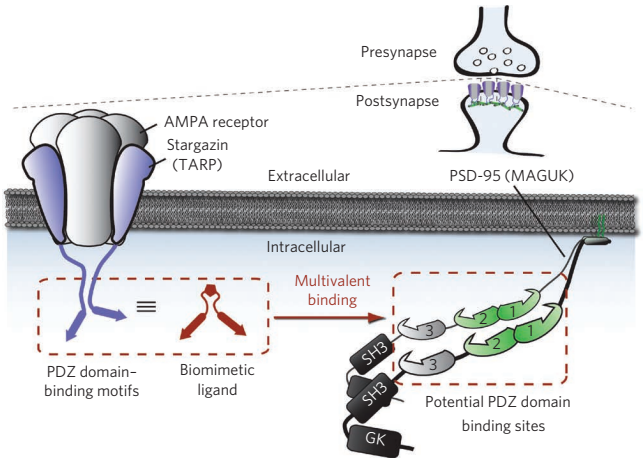

Figure 1 | Role of multivalency in the stabilization of AMPAR–Stargazin complex interactions with PSD-95 (working model) and implication for the development of chemical-based perturbating tools. Three major aspects of the supramolecular assemblies are likely sources of multivalent interactions. (i) Multiple PDZ domain–binding motifs. The AMPAR–Stargazin complex is composed of four subunits encoded by the glutamate receptor gene arranged as homo- or heterotetrameric channels[1] and incorporates several TARPs as auxiliary subunits. The complex organization results in the clustering of multiple class I PDZ domain–binding motifs from the cytosolic C terminus of TARPs. (ii) Multiple PDZ domains per MAGUK. Synaptic MAGUKs are characterized by a repeat of three PDZ domains, which are regrouped on the N-terminal portion of the protein[13]. All three domains are similar in sequence and can engage interactions with binding partners displaying X-S/T-X-**Φ** (**Φ**: aliphatic amino acid) as a C-terminal class I consensus sequence[14,15]. The supramodular assembly comprising the first two PDZ domains of PSD-95 shows a preorganization of the two domains that favors interactions with multivalent binding partners[16]. (iii) MAGUKs clustering. The N-terminal motif of PSD-95, which undergoes palmitoylation, is responsible for the protein dimerization or multimerization[17]. These oligomerizing properties, which are critical for AMPAR activity[17], result in a further clusterization of PDZ domains. Synthetic ligands that mimic the preoganization of multiple PDZ domain–binding motifs (for instance, biomimetic ligands) should bind tightly to clustered PDZ domains and be efficient at disrupting the native interactions of the AMPAR complex with PDZ domain–containing scaffold proteins.

and in particular include a repeat of three clustered class I PDZ domains[14,15] that provide anchoring sites for multiple binding partners[13]. Furthermore, the relative orientation of the ligand-binding grooves of the first two PDZ domains of PSD-95 favors accommodating multiple ligands originating from the same face, according to a NMR-derived structural model[16]. Functional studies in neurons indicate that the AMPAR–Stargazin complex preferentially binds to either or both of the first two PSD-95 PDZ domains[4,17]. Finally, the oligomerization properties of MAGUKs add another degree of complexity that allows for multivalent interactions. In particular, PSD-95α (predominant in neurons[18]) can form dimeric or multimeric assemblies via the N-terminal region[17]. Notably, this property is critical for the AMPAR's synaptic function, as mutants that prevent oligomerization show effects on basal AMPAR currents[4,17].

Here, we describe a chemically based approach to disrupt AMPAR synaptic stabilization. Taking into consideration a working model in which multiple Stargazins from an AMPAR complex bind simultaneously to clustered MAGUK PDZ domains, we developed a synthetic strategy for generating biomimetic divalent ligands that replicate the native interactions and address the issue of multivalency (**Fig. 1**). By combining biophysical methods and studies in heterologous cells, we show that Stargazin-derived divalent ligands have an enhanced affinity for clustered MAGUK PDZ domains while maintaining a specificity comparable to the parent protein. In cultured neurons, the biomimetic ligands acutely disrupt the AMPAR–Stargazin–PSD-95 interaction, as shown by significant effects on AMPAR mobility and currents. In addition to providing evidence of a role for multivalency in AMPAR synaptic stabilization, these data demonstrate the efficiency of the biomimetic tools.

RESULTS

PSD-95 tandem PDZ domains and design of divalent ligands

To guide the design of divalent biomimetic ligands for perturbing the AMPAR–Stargazin–PSD-95 interaction, we solved the X-ray crystal structure of the tandem PDZ domains of PSD-95 (domains 1 and 2, PDB: 3GSL). Initial attempts with a minimal construct (PSD-95-1+2) yielded only poorly diffracting crystals; therefore, we engineered a construct in which we appended the last four residues of a binding motif derived from GluK2 (GluR6), -ETMA, which associates specifically to PSD-95-1 with a modest affinity, to the C terminus of the tandem motif construct[19,20]. Because a similar approach had been used to aid the crystallization of individual PDZ domains[21], we anticipated a stabilization of the tandem domains with respect to each other, owing to the C-terminal binding motif of one molecule targeting the N-terminal domain of the other. The spacer length between the C terminus of PSD-95-2 and the GluK2 binding motif was varied from zero to four residues to screen for optimal protein packing. The shortest linker chimera produced crystals diffracting to 2.0-Å resolution. The tandem structure was solved by molecular replacement using the X-ray crystallographic structures of the two individual PDZ domains of SAP102.

The structure reveals two tandem domain protomers per asymmetric unit (**Fig. 2a** and **Supplementary Figs. 1** and **2**). Each protomer interacts via the C-terminal extension, harboring the GluK2 binding motif, with the N-terminal PDZ domain (domain 1) of an adjacent protomer. In general, all of the individual domains adopt the canonical PDZ domain tertiary fold[22,23] (**Supplementary Fig. 1a**). In regards to the supramodular unit composed of the two PDZ domains, the X-ray structure is consistent with a previously reported NMR model[16]. For each protomer in the asymmetric unit, the PDZ domains are oriented in a manner that can easily accommodate multivalent binding partners originating from the same direction by exposing their binding grooves in an antiparallel manner on the same face of the protein (**Fig. 2b**). Notably, although the structure of each individual domain was robustly conserved, the relative positions of domains 1 and 2 varied significantly for the two protomers. This indicates a conformational flexibility that arises from a short flexible linker (-KPPAE-) and minimal interdomain 'contacts'. This interpretation is consistent with recent NMR studies in which conformational flexibility for the PSD-95 tandem structure is observed for both the unbound and the bound domains, albeit with a much larger amplitude with the binding of ligands[24]. Next, considering the flexibility of the PSD-95 tandem PDZ domains, we used the structure to establish the distance between the PDZ domain binding grooves in order to design divalent ligands. By modeling ligands into the binding grooves, we estimated that approximately 16–18 amino acids would be required to allow for simultaneous binding to the two domains (**Fig. 2c**). We therefore developed a panel of divalent ligands composed of 10-, 15- and 20-residue long monomeric units derived from the C-terminal Stargazin sequence in order to obtain probes that would ensure sufficient length and flexibility while preserving specificity determinants of the native sequence.

Synthesis of divalent PDZ domain ligands

The synthesis of divalent PDZ domain ligands requires an approach in which the monomer unit ligation occurs at the N terminus, to preserve the unmodified C-terminal motifs for binding. Therefore, we used a general strategy in which the ligation was performed

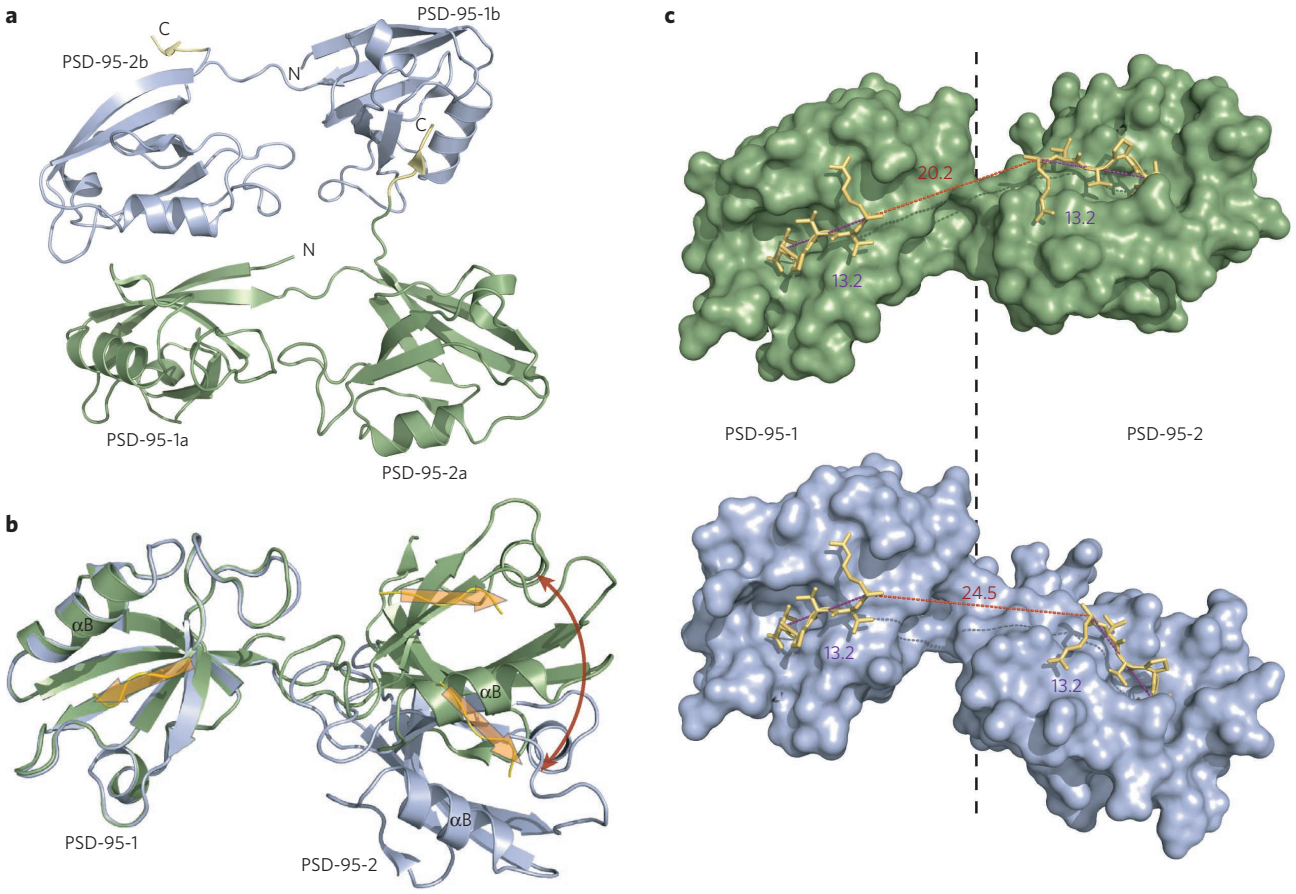

Figure 2 | Structure of the tandem PDZ domains of PSD-95 (domains 1 and 2, PDB: 3GSL). (**a**) Ribbon representation of the two self-binding tandem domains constituting the asymmetric unit with chain 'a' in green, chain 'b' in light blue and the appended domain 1 ligand, -ETMA, from the GluK2 (GluR6) binding motif in yellow on both chains. (**b**) Superposition of the two tandem PDZ domains (chain 'a' in green and chain 'b' in light blue). Alignment was performed on PSD-95-1a and PSD-95-1b of the two tandem structures to show the conformational flexibility of the supramodular ensemble. The PDZ domain binding grooves are highlighted with arrows, and the α-carbon chain of modeled ligands is represented in yellow. (**c**) Estimation of the distance between the PDZ domain binding grooves (surface representation, colors as in panel **b**). For both chains, the last five residues of the Stargazin binding motif (-RTTPV, in yellow ribbon and lines) were docked into each PDZ domain binding groove by alignment with a structure of the ligand complexed with a homologous PDZ domain (PDB: 3JXT). Distances (reported in angstroms) were measured between the Cα of the ligand residues at positions 0 and −4 (purple) and between the Cα of the residues at the −4 position of the two ligands (in domain 1 and 2, red).

using a Cu(I)-catalyzed Huisgen 1,3-dipolar cycloaddition[25], or click chemistry, approach. This method is versatile, allows the coupling of monomeric units at various stages of the synthesis and is compatible with the design of symmetrical as well as asymmetrical multivalent peptides. The approach also benefits from its orthogonality with respect to standard solid phase peptide synthesis (SPPS) conditions and natural amino acid functional group reactivity. The general method involves (i) synthesis of peptide monomeric ligands using Fmoc-based SPPS; (ii) elongation at the N terminus with a mixture of 4-pentynoic acid and an azide-derived acid (azido acetic acid, Fmoc-Lys[N_3]-OH or Fmoc-Dab[Alloc]-OH); and (iii) on-resin ligation of alkyne- and azide-derived peptides in the presence of a catalytic amount of Cu(I) to afford the 1,3-triazole–containing divalent ligands (**Scheme 1** and **Supplementary Figs. 3–7**).

As the goal was to mimic the native AMPAR–Stargazin–PSD-95 interactions, we based the monomeric peptide sequences on the native Stargazin C-terminal motif. Furthermore, given the similar affinity of this motif for domains 1 and 2 of PSD-95 (ref. 26), we prepared homodimeric ligands, although, in principle, a modification of the synthetic method could be used to prepare analogous heterodimeric ligands. In addition, for comparison purposes we synthesized the corresponding monovalent peptides and control divalent ligands in which critical residues were replaced by arginine residues to prevent PDZ domain binding[27].

Overall, three series of ligands were synthesized for the different goals of this study (**Fig. 3** and **Supplementary Table 1**). First, for the *in vitro* characterization of the interaction with PSD-95 tandem PDZ domains, the ligands incorporated the 4-dimethylaminophthalimide (4-DMAP) environment-sensitive fluorophore[28] and were designed with different monomeric unit lengths in order to quantitatively assess the optimal binding ligand. The site of ligation of the monomeric units, which defines the overall length of the dimer, was varied by increments of five amino acids, on the basis of evaluation of the distance between domain 1 and 2. Thus, the resulting dimers included monomer units of 10, 15 and 20 amino acids respectively. We have recently shown that the fluorescence increase of an appropriately positioned 4-DMAP chromophore within a peptide sequence can be used to directly report binding to PDZ domains with minimal interference and hence provides reliable determination of affinity constants[27]. The solvatochromic fluorophore was inserted at the −5 position with a diaminobutyric acid linker, which was the most efficient for observing a fluorescence increase with the tandem PDZ domains of PSD-95 (ref. 27). Next, for biophysical studies and electrophysiology experiments in primary neuron

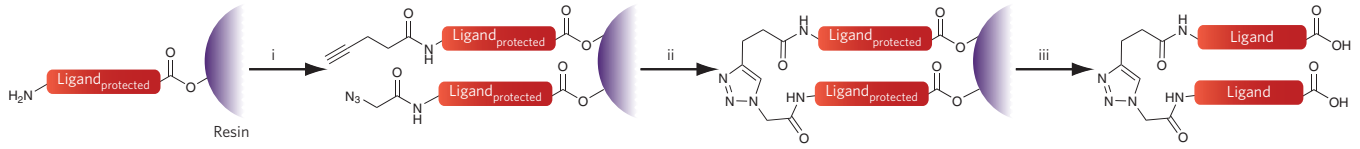

Scheme 1 | General synthesis scheme for divalent peptide-based ligands. (i) Pentynoic acid/azidoacetic acid (3:4), HBTU (O-(benzotriazol-1-yl)- *N,N,N′,N′*-tetramethyluronium hexafluorophosphate)/HOBt (1-hydroxy-benzotriazole), DIPEA (*N,N*-diisopropylethylamine), DMF (*N,N*-dimethylformamide); (ii) Copper iodide, ascorbic acid, 4-methylpiperidine/DMF (2:8); (iii) cleavage cocktail.

cultures, a series of Stargazin-based divalent ligands was developed with the optimal linker length. Finally, for the other cellular experiments, a series of cell-permeable ligands was developed by coupling the previous series of ligands to a protein transduction domain, the HIV-1 TAT sequence (TAT_{47-57})[29,30]. The coupling was achieved in the later steps of the synthesis by native chemical ligation[31,32].

Characterization and selection of divalent ligands

The optimal length for divalent ligands that mimic two Stargazin proteins complexed to an AMPAR was chosen on the basis of biophysical studies of the PSD-95 tandem PDZ domains using fluorescence-based assays. Although the approach focused on the tandem domains as the simplest form of divalent interaction, because the Stargazin binding motif interacts equally well with both domains[26], we also considered the potential for the N-terminal oligomerization of PSD-95 for AMPAR activity[17]. Therefore, we sought to include in the analysis the possibility of 'intertandem' interactions by maintaining a system that mimicked N-terminal motif clustering properties. In the absence of a detailed understanding of the nature of the native interactions, this approach enables the ligands to adapt to the most favored mode of interaction and thus decreases the risk of a biased selection against an oversimplified system. In this context, we chose to exploit the intrinsic dimerizing properties of the GST coexpression tag[33] in order to obtain a construct that mirrors the N-terminal clustering of PSD-95 for the tandem PDZ domains (GST-PSD-95-1+2).

Two aspects of the design were considered in the fluorescence-based studies: first, a comparison between monovalent and divalent ligands, and second, the optimal distance between the two ligand units required for binding. The fluorescence titrations (**Fig. 4a**) clearly revealed the superior affinity of divalent over monovalent ligands with K_D values in the low micromolar range for the monomer and in the submicromolar range for the dimers. This indicates that divalency improves the binding efficiency by increasing the effective concentration of ligand. The dissociation constants of the divalent ligands varied with the overall length of the linker, and

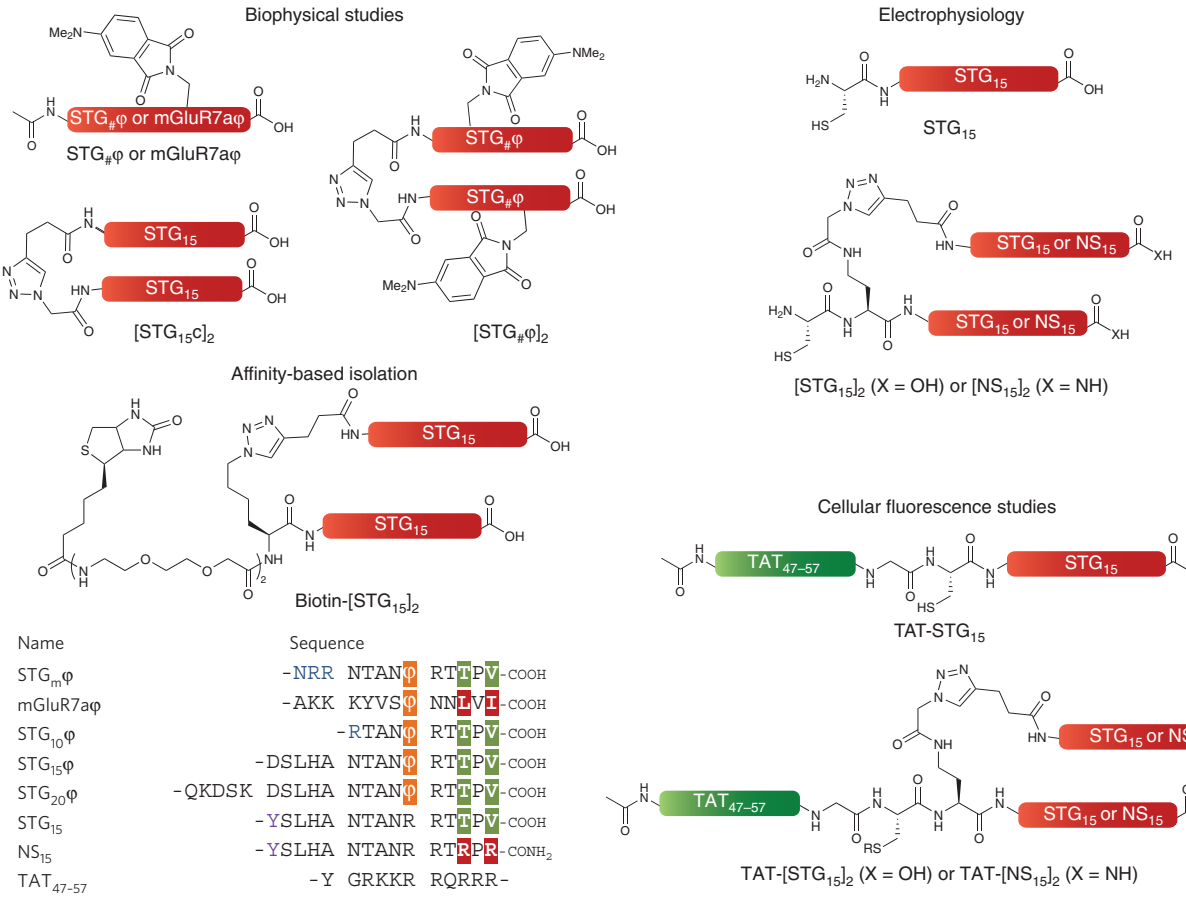

Name	Sequence
$STG_m\varphi$	-NRR NTAN(φ) RTTPV-COOH
mGluR7aφ	-AKK KYVS(φ) NNLVI-COOH
$STG_{10}\varphi$	-RTAN(φ) RTTPV-COOH
$STG_{15}\varphi$	-DSLHA NTAN(φ) RTTPV-COOH
$STG_{20}\varphi$	-QKDSK DSLHA NTAN(φ) RTTPV-COOH
STG_{15}	-YSLHA NTANR RTTPV-COOH
NS_{15}	-YSLHA NTANR RTRPR-CONH2
TAT_{47-57}	-Y GRKKR RQRRR-

Figure 3 | Structure of the monovalent and divalent ligands. #: 10, 15 or 20. φ: Dab(4-DMAP). R: Hydrogen or BODIPY-FI-maleimide. Critical residues at positions 0 and −2 are highlighted (green for the common residues found in PSD-95 ligands, red otherwise); residues in blue and purple were added for solubility and quantification purposes respectively.

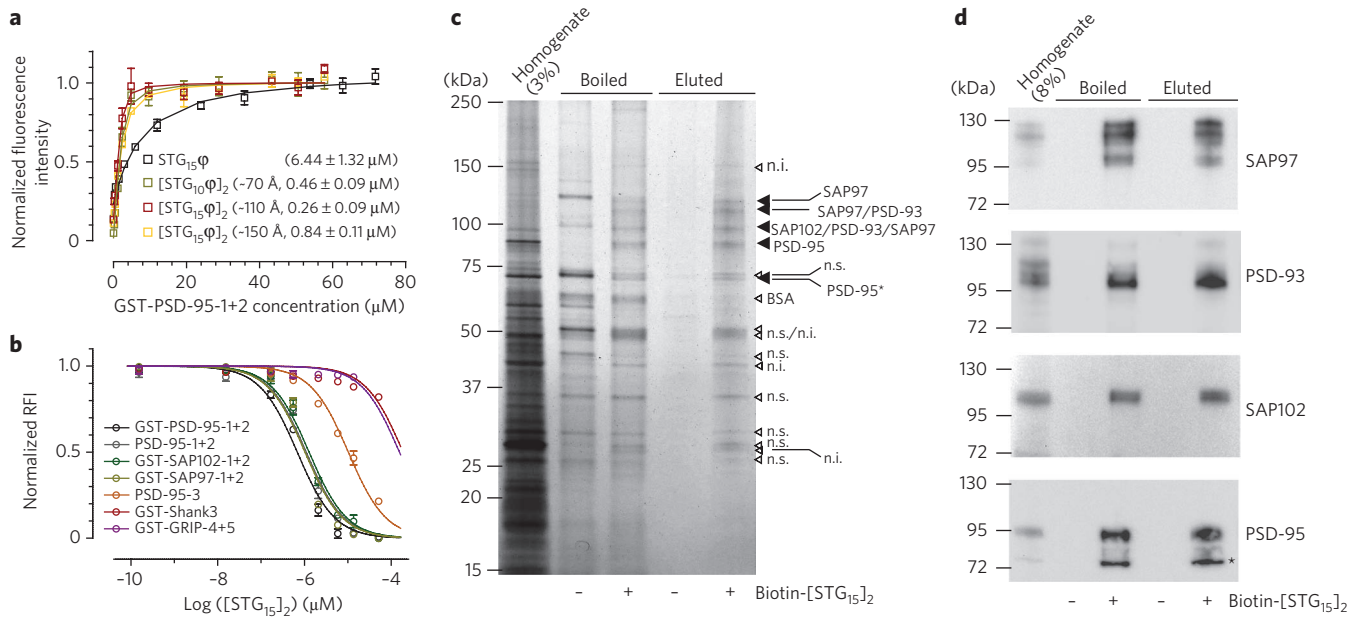

Figure 4 | Characterization of the peptide-based ligand interactions with PDZ domains. (**a**) Fluorescence titrations of monovalent (4.8 μM) and divalent (2.4 μM) fluorescent Stargazin-derived ligands against GST-PSD-95-1+2 (averaged normalized fluorescence intensity ± s.e.m. and fitting curve, $n \geq 3$). The affinity constants are reported as $K_D \pm$ s.d. in micromolar units in parenthesis together with an estimation of the overall length of the divalent ligands. (**b**) Competitive titrations of the selected nonfluorescent divalent ligand with optimal length, $[STG_{15}c]_2$, against a fluorescent monovalent ligand (1.9 μM, $STG_m\varphi$ or mGluR7aφ for class II PDZ domains of GRIP[27]) complexed to various PDZ domain constructs (2.0 μM, averaged normalized relative fluorescence increase ± s.e.m. and fitting curve, $n \geq 3$). Refer to **Supplementary Table 2** for the affinity constants. (**c**) Isolation of the protein targets of the Stargazin-derived divalent ligand from unfractionated adult rat brain homogenates. Silver staining of affinity-precipitated proteins separated by SDS-PAGE and tentative assignment of bands (n.s.: nonspecific, meaning the band was also observed in the absence of biotin-$[STG_{15}]_2$; n.i.: nonidentified potential target; PSD-95*: PSD-95 degradation product). Both methods used for protein release—boiling in SDS ("Boiled") or elution with a nonbiotinylated divalent ligand ("Eluted")—are associated with the presence of nonspecific signal attributed to nonspecific binding of proteins to the beads or streptavidin and MAGUK coprecipitates. (**d**) Western blot analysis of affinity-precipitated proteins with antibodies for the four postsynaptic MAGUKs. For both **c** and **d**, biotin-$[STG_{15}]_2$ was used at 1 μM (similar results were obtained at higher concentration, see **Supplementary Fig. 9**).

the optimal dimer was the intermediate-length ligand, $[STG_{15}\varphi]_2$, with 15 amino acids per single binding motif. The lower efficiency of the other divalent ligands suggests that the shorter construct ($[STG_{10}\varphi]_2$) cannot efficiently reach the two binding domains, whereas the longest divalent ligand ($[STG_{20}\varphi]_2$) may be negatively affected by an increase in entropy. If the effect of multivalency was solely the consequence of increased concentration, then the trend in ligand binding would not be expected to be so profoundly influenced by linker length. Our results are therefore consistent with simultaneous binding of the two motifs. Finally, the most efficient divalent ligand had a significantly improved affinity with a K_D value more than 25-fold lower than the corresponding monovalent parent. In light of these results, we therefore chose to further develop divalent ligands based on the 15-residue sequence, the construct $[STG_{15}]_2$, for cellular studies.

Specificity of the Stargazin-derived divalent ligand

In light of the overall length of the dimeric ligand with respect to the structure of the tandem domains, we considered the possibility of intertandem versus intratandem binding. Competitive titrations with a nonfluorescent divalent ligand ($[STG_{15}c]_2$, **Fig. 4b**) showed only a modest decrease in affinity for a nondimerizing PSD95-1+2 construct when compared to GST-PSD-95-1+2. Moreover, dynamic light-scattering studies (**Supplementary Fig. 7**) did not show evidence for a higher order complex involving cross-linking of $[STG_{15}c]_2$ with PSD95-1+2. Thus, an intratandem mode of binding does not appear to prevail in our system. We then evaluated the specificity of the divalent ligand based on the 15-residue binding motif of Stargazin with other synaptic PDZ domains by competition-based binding assays (**Fig. 4b** and **Supplementary Table 2**). The affinity of $[STG_{15}c]_2$ for other tandem PDZ domains from related MAGUKs (SAP97 and SAP102) was only modestly diminished in comparison to that observed for PSD-95, which is consistent with the high levels of sequence homology for the PDZ domains of that protein family (**Supplementary Fig. 8**) and reports of such interactions from Stargazin in yeast two-hybrid assays[34,35] and in neurons for SAP102 (refs. 4,36). In contrast, the K_I for the isolated third PDZ domain of PSD-95, as an identified class I partner of the minimal Stargazin C-terminal motif *in vitro*[26,27], was increased by more than ten-fold. Furthermore, both the class I Shank3 and the tandem class II GRIP PDZ domains showed more than a 250-fold decrease in affinity. Finally, to further assess the specificity of the probe, we applied an affinity-based approach to isolate the protein targets from a whole-brain homogenate. The proteins specifically pulled down by the $[STG_{15}]_2$ probe primarily composed a cluster of proteins in the 130–90 kDa range that could be attributed to the four synaptic MAGUKs, on the basis of immunoblotting analysis (**Fig. 4c**,**d** and **Supplementary Fig. 9**). Additional species were also observed at ~150, ~50, ~45 and ~28 kDa, respectively, which could either be alternative targets, MAGUK coprecipitates or degraded MAGUKs. Overall, these results clearly suggest a strong specificity of the divalent Stargazin-derived ligands toward the tandem PDZ domains of PSD-95–like MAGUKs.

FRET-FLIM studies in the cellular environment

Next, we characterized the optimized ligands with the Stargazin–PSD-95 interaction using full-length proteins in transfected

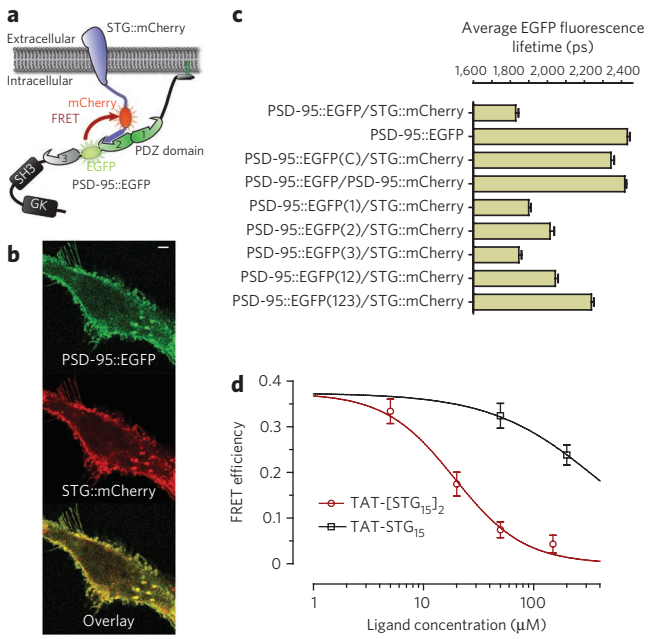

Figure 5 | FRET-FLIM system for the characterization of the interactions between the divalent ligand and the Stargazin–PSD-95 complex in live cells. (**a**) FRET system between Stargazin and PSD-95. The fluorescence acceptor, mCherry, was inserted at position −21 on the cytosolic tail of Stargazin, thus preserving the PDZ domain–binding motif (STG::mCherry). The donor, EGFP, was introduced between the second and third PDZ domains of PSD-95 to allow for monitoring of binding with all three domains (PSD-95::EGFP). In both cases, the fluorescent proteins were incorporated in regions that lacked secondary structure to minimize interference with the native interaction. (**b**) Confocal images of cotransfected COS-7 cells (scale bar: 2 μm). (**c**) Average EGFP fluorescence lifetime (± s.e.m., $n \geq 10$) measured in live COS-7 cells (see **Supplementary Fig. 11** for the corresponding FRET efficiencies). (**d**) Titration of the effect of the monovalent and divalent ligands on the STG::mCherry/PSD-95::EGFP interaction (average ± s.e.m., $n \geq 17$). EC_{50} = 19.1 μM and 375 μM for TAT-STG_{15} (red) and TAT-$[STG_{15}]_2$ (black), respectively.

eukaryotic cells as a model for a complex cellular system. Specifically, we developed a fluorescence resonance energy transfer (FRET)–based assay with EGFP and mCherry as a fluorescent protein pair inserted into PSD-95 and Stargazin, respectively (**Fig. 5a**). Additional constructs, including FRET controls and PDZ domain–defective mutants of PSD-95, were also designed and examined (**Supplementary Fig. 10**). The fluorescent fusion proteins were cotransfected into COS-7 cells, and FRET efficiency was assessed in live cells by measuring the variation in the donor fluorescence lifetime (FLIM) as a function of acceptor proximity (**Fig. 5b,c** and **Supplementary Fig. 11**). In the absence of acceptor, EGFP fluorescence average lifetime was characterized by a mono-exponential emission decay of ~2.4 ns, whereas for the STG::mCherry and PSD-95::EGFP system (where :: denotes a fusion between two proteins), approximately 30% of the EGFP population had a shorter lifetime (~1.5 ns), consistent with results obtained with a control EGFP::mCherry tandem. In contrast, lack of FRET signal observed with the cotransfection of controls (PSD-95::EGFP and PSD-95::mCherry or STG::mCherry and PSD-95::EGFP(C)) indicated that FRET is resulting from specific interactions between Stargazin and PSD-95. Next, PDZ domain mutants were used to determine the domains targeted by Stargazin. Each domain was therefore converted from a class I to a class II PDZ domain by mutating a conserved histidine residue in each domain into a valine[4,14,15]. All single-domain mutants afforded a decrease of FRET, with a stronger effect from the mutated second domain, and this effect was cumulative for double and triple mutants. Together, these experiments indicate that the Stargazin-PSD-95 interaction is driven by the three PDZ domains, in agreement with studies of the Stargazin binding motif with the isolated recombinant domains[26,27]. The preorganization of TARPs by AMPARs or the presence of other ligands, absent in our model system, might account for more selective binding of Stargazin in native environment; this possibility does not allow for a simple transposition of the results of this study to the more complex neuronal system.

Monovalent and divalent nonfluorescent cell-permeable ligands (TAT-STG_{15} and TAT-$[STG_{15}]_2$) were then incubated with cotransfected cells at various concentrations, and the efficiency of displacing the Stargazin interaction was assessed by monitoring the decrease of FRET efficiency in live cells. First, control experiments confirmed the efficient delivery of the probe into the cytosol and binding to PSD-95 PDZ domains (**Supplementary Fig. 12a**). Both TAT-STG_{15} and TAT-$[STG_{15}]_2$ showed a dose-dependent effect, with a decrease of FRET efficiency as a result of an increase in ligand concentration (**Fig. 5d**). In contrast, the control divalent ligand, TAT-$[NS_{15}]_2$, did not show any effect up to 50 μM (**Supplementary Fig. 12b**), thus confirming that the activity of the ligands is resulting from specific interactions with the targeted PDZ domains. TAT-$[STG_{15}]_2$ was significantly more efficient at binding to PSD-95 and displacing Stargazin than the monovalent parent was. The divalent, but not monovalent, PDZ domain ligand had strong cooperative interaction with PSD-95, with Hill coefficients of 1.4 (TAT-$[STG_{15}]_2$) and 0.9 (TAT-STG_{15}). Most importantly, consistent with the *in vitro* studies, the half-maximal effective concentration (EC_{50}) analyses revealed a ~20-fold increase of efficiency as a result of the ligand divalency. Overall, the FRET-FLIM studies validated the ligand selection process and demonstrated the efficiency of the divalent ligands in perturbing interactions in a complex cellular system.

Effect of biomimetic ligands on AMPAR surface mobility

Using a 24–48 h overexpression of mutant Stargazin, we previously established that the interactions between the Stargazin C-terminal PDZ domain–binding motif and PSD-95 PDZ domains control the lateral diffusion of AMPARs at the neuronal plasma membrane and are required for the trapping of AMPARs at postsynaptic sites[3]. We thus investigated whether TAT-$[STG_{15}]_2$ could compete for endogenous TARP-MAGUK interaction and modulate AMPAR mobility on the level of minutes by single-particle tracking of quantum dot–labeled AMPARs. Fluorescent derivatives of TAT-$[STG_{15}]_2$ and TAT-$[NS_{15}]_2$ were taken up by cultured hippocampal neurons within a few minutes and showed a somatodendritic distribution with well-resolved dendritic spines (**Supplementary Fig. 13**). Incubation for 5 min with 5 μM TAT-$[STG_{15}]_2$, but not with TAT-$[NS_{15}]_2$, induced a rapid increase in GluA2-containing AMPAR mobility in both synaptic and extrasynaptic domains (**Fig. 6a** and **Supplementary Fig. 14**), as shown by the increased surface area explored by the receptor and the corresponding increased slope of the mean square displacement (MSD) versus time plot in presence of TAT-$[STG_{15}]_2$. Similarly, the distribution of diffusion coefficients showed a near-complete loss of the immobile fraction of AMPARs (**Fig. 6b**) with a markedly increased median diffusion rate in the presence of TAT-$[STG_{15}]_2$ (**Fig. 6c**). Such an effect was not observed for Kv1.3-containing Shaker-type potassium channels (**Supplementary Fig. 15**), which are clustered by PSD-95 tandem PDZ domains[37,38]. The divalent ligand-induced increase in AMPAR mobility was only transient, peaking at around 4–5 min (synaptic and extrasynaptic mobile fractions, TAT-$[STG_{15}]_2$: 55.51 ± 3.23% and 88.21 ± 2.74%; control: 33.94 ± 5% and 62.96 ± 5.9%) and disappeared 10 min after application of the ligand (**Fig. 6d**). We attribute the extrasynaptic increase in mobility to both the release of AMPAR complexes from the PSD and the competition of extrasynaptic Stargazin-MAGUK

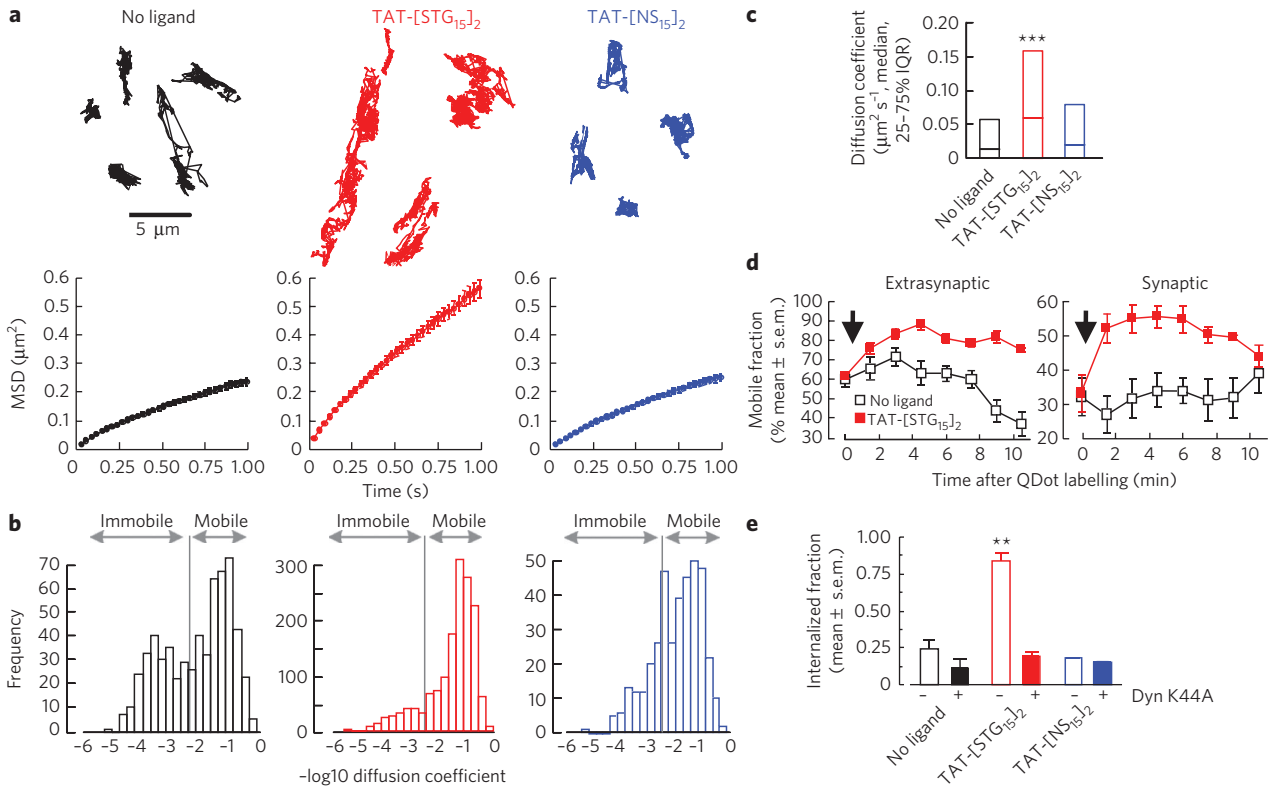

Figure 6 | TAT-$[STG_{15}]_2$ induces a rapid and transient increase in the surface mobility of GluA2-AMPARs. (**a**) Sample trajectories (top) and average MSD versus time curves (bottom) for quantum dot (QDot)-labeled GluA2-AMPARs, under control condition (no ligand, $n = 604$ trajectories), or after 5 min incubation with 5 µM TAT-$[STG_{15}]_2$ ($n = 1{,}000$ trajectories) or TAT-$[NS_{15}]_2$ ($n = 942$ trajectories). (**b**) Diffusion coefficient distributions for data in **a**; cut-off value for mobile receptors: 0.003 $\mu m^2\ s^{-1}$. (**c**). Summary of the diffusion coefficients in **a** and **b**. TAT-$[STG_{15}]_2$: 0.059 $\mu m^2\ s^{-1}$, IQR = 0.021–0.16 $\mu m^2\ s^{-1}$; TAT-$[NS_{15}]_2$: 0.027 $\mu m^2\ s^{-1}$, IQR = 0.0149–0.074 $\mu m^2\ s^{-1}$; control: 0.018 $\mu m^2\ s^{-1}$, IQR = 0.049–0.11 $\mu m^2\ s^{-1}$; $^{***}P < 0.01$ versus control, one-way ANOVA. (**d**) Time course of mobile AMPAR fraction during continuous extracellular presence of 5 µM TAT-$[STG_{15}]_2$ ($n = 7$ cells) or control (no ligand, $n = 8$ cells); ligands were added to the bath solution immediately after the first acquisition epoch (arrows). (**e**) Fraction of internalized GluA2-AMPARs under control (no ligand, $n = 5$ cells), or after 10 min incubation with 5 µM TAT-$[STG_{15}]_2$ ($n = 6$ cells) or 5 µM TAT-$[NS_{15}]_2$ ($n = 5$ cells); $^{**}P < 0.01$ versus control, two-tailed Mann-Whitney U test.

interactions. A similar mobility trend was previously observed with the expression of dominant negative Stargazin-ΔC[3]. In addition, we reasoned that the transient effect might be because of the entry of mobile AMPARs freed from their PSD-95 anchor in the endocytic pathway, in which they would appear as immobile[39]. Measuring AMPAR endocytosis by an antibody-based assay, we indeed found that 10-min incubation with TAT-$[STG_{15}]_2$, but not TAT-$[NS_{15}]_2$, induced a marked increase in the fraction of constitutively internalized AMPARs (**Fig. 6e**). This effect was blocked by the GTPase dominant-negative mutant dynamin2 K44A[40], indicating that it occurs via a dynamin2-mediated endocytic pathway.

Effect of biomimetic ligands on synaptic AMPAR currents

We next investigated the effect of the Stargazin-based ligands on synaptic AMPAR currents evoked in pairs of monosynaptically coupled cultured hippocampal neurons[41]. Inclusion in the postsynaptic patch pipette of 50 µM $[STG_{15}]_2$, but not STG_{15} or $[NS_{15}]_2$, induced a progressive rundown of AMPAR-mediated EPSCs, reaching an equilibrium after 15–20 min at 45 ± 4% of the current amplitudes during the first minute of recording (**Fig. 7a**). There was no significant EPSC rundown in controls with no ligand or, more importantly, with monovalent STG_{15}. At lower concentrations of $[STG_{15}]_2$ (5 µM), the AMPAR EPSC inhibition developed more slowly but reached a similar equilibrium: at 40–45 min recording time, amplitudes were down to 48 ± 3% and 47 ± 8% of the initial values, for 5 µM and 50 µM $[STG_{15}]_2$, respectively (**Fig. 7a**). In contrast, intracellular dialysis with 50 µM $[STG_{15}]_2$ did not affect the *N*-methyl-D-aspartate (NMDA) receptor EPSCs over 30 min of recording (5-min average EPSC amplitudes at 5, 15 and 30 min: 226 ± 60.29, 213.34 ± 56.32, 194.25 ± 72.98 picoamps (pA), **Fig. 7b**). Reciprocally, a divalent ligand derived from the C-terminal 15 residues of the NMDA GluN2A subunit had no effect on the AMPAR EPSCs (**Supplementary Fig. 16**). As an alternative evaluation of the effect of the Stargazin-derived ligand on synaptic transmission, we recorded spontaneous AMPAR-mediated miniature EPSCs (mEPSCs). Intracellular dialysis of $[STG_{15}]_2$, but not $[NS_{15}]_2$, induced a rundown of mEPSCs as soon as 5 min (−38.92 ± 0.68 pA versus −51.5 ± 0.7 pA in the first minute of recording, **Fig. 7c**). This effect also equilibrated rapidly (**Fig. 7d**). The ligands had no effect on either the decay kinetics (**Fig. 7e**) or the frequency of the mEPSCs (**Fig. 7f**).

DISCUSSION

Perturbation of the AMPAR complex dynamics at the PSD has thus far principally been achieved by preventing expression of either Stargazin or PSD-95 (ref. 17) or by the use of mutants that impair either the PDZ domain–mediated interaction[3,4] or the proper function of PSD-95 (ref. 17). Although these approaches have greatly contributed to the understanding of the molecular mediators of AMPAR trafficking, the detailed molecular mechanisms and the regulation processes that govern AMPAR transport and retention at the synapse have yet to be elucidated. We report herein the first set of chemical tools capable of acutely disrupting AMPAR synaptic anchoring, thus enabling studies on endogenous protein populations with a high level of temporal control.

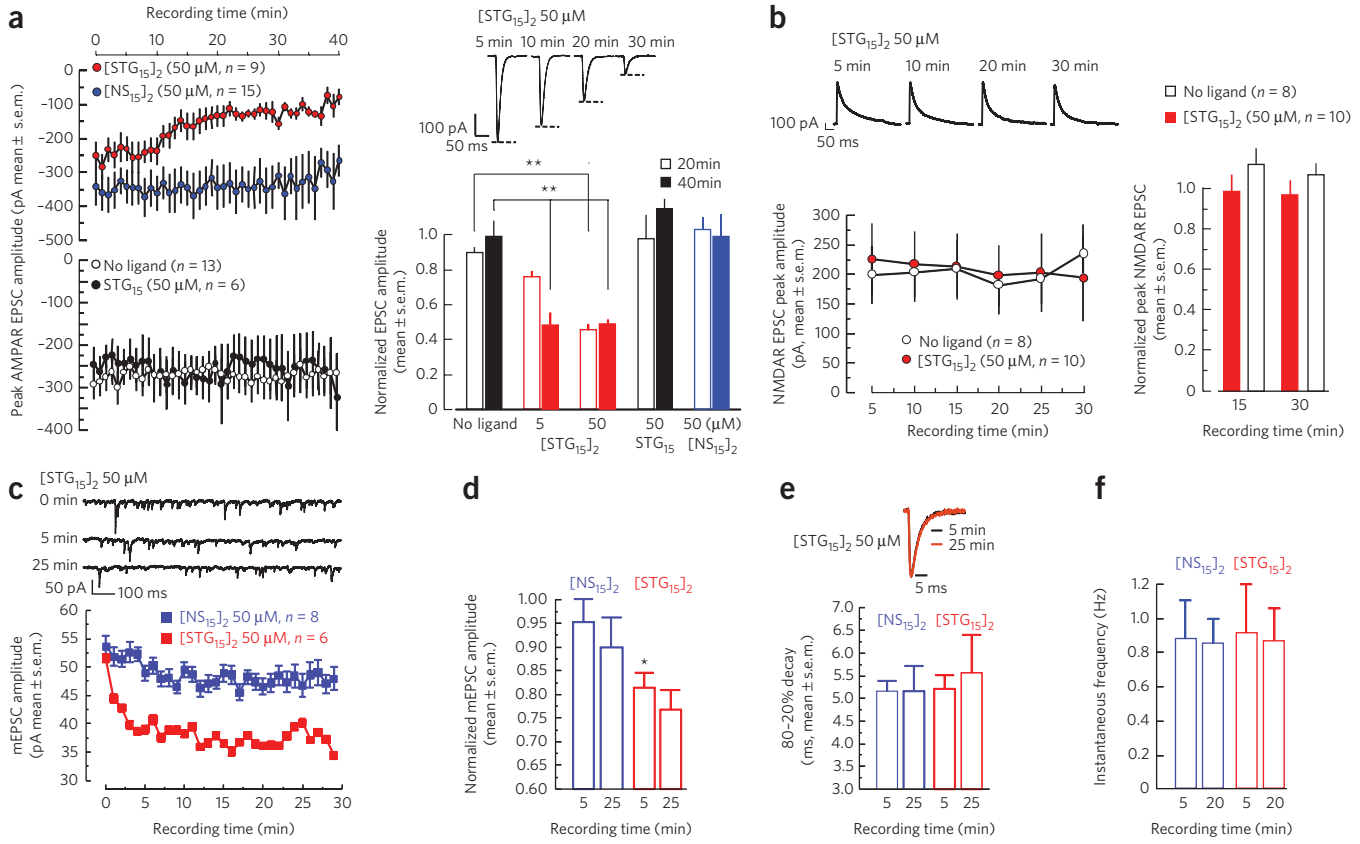

Figure 7 | Effect of intracellular $[STG_{15}]_2$ on AMPAR synaptic currents. (**a**,**b**) Inhibition of evoked AMPAR EPSCs by intracellular $[STG_{15}]_2$. (**a**) Left: Time course of evoked AMPAR EPSCs in monosynaptically coupled cultured hippocampal neurons. Top right: Sample AMPAR EPSCs from a cell dialyzed with $[STG_{15}]_2$. Bottom right: Summary of AMPAR EPSC amplitudes normalized to the first minute of recording; $^{**}P < 0.01$ versus no ligand control, unpaired *t*-test. (**b**) Time course of evoked NMDAR EPSC in synaptically coupled cultured hippocampal neurons (bottom), with sample recordings (top) and summary of amplitudes normalized to the first minute of recording (left); ligand concentrations in the pipette solution and the number of cells for each condition are shown in parenthesis. (**c**–**f**) Intracellular $[STG_{15}]_2$ induces a rundown of AMPAR mEPSC. (**c**) Time course of AMPAR mEPSC amplitude for cells dialyzed with divalent Stargazin-derived ligand ($[STG_{15}]_2$) or control ligand ($[NS_{15}]_2$); top traces: sample mEPSC recordings from a $[STG_{15}]_2$ cell. (**d**) Summary of mEPSC amplitudes normalized to the first minute of recording, for the data in **c**; $^{*}P < 0.1$, *t*-test. (**e**) Summary of AMPAR mEPSC decay time constants for the cells in **a**; top inset: scaled and overlaid mEPSC waveforms, averaged over one minute, taken from a $[STG_{15}]_2$-dialyzed cell at 5 min (black) and 25 min (red) recording time. (**f**) Instantaneous frequency (reciprocal of the mean interval) of mEPSCs in **c**. Data in **c**–**f** represent a 5-min time window around 5 and 25 min of recording.

The studies in rat hippocampal neurons clearly show that the Stargazin-derived divalent ligands effectively disrupt AMPAR complexes from the PSD. This is attributed to the capacity of the ligands to directly compete with the native TARP-MAGUK PDZ domain–mediated interactions, as indicated by both the ineffectiveness of a mutated control ligand (-$[NS_{15}]_2$) and the nature of the observed effects, which are comparable to the changes obtained with overexpression of mutated Stargazin for which binding to the PDZ domain is impaired[3,4]. Notably, in contrast to related studies[5–7], the monovalent ligand failed to show significant effect on AMPAR currents, even at concentrations ten times the K_D measured for PSD-95 tandem PDZ domains. In light of these observations, the difference in efficiency of divalent versus monovalent ligand can be attributed either to a tighter binding of the full-length TARP C-terminal sequence to its synaptic scaffold target in comparison to minimal peptides or a multivalent stabilization of the AMPAR–TARP–MAGUK complex. The *in vitro* studies indicate that the key residues for the interaction of Stargazin with PSD-95 PDZ domains do not extend beyond the last 15 amino acids, thus supporting the role of multivalency. The validity of this model is strongly underscored by the observed beneficial effect of tethering two Stargazin binding motifs to increase the affinity for multiple PDZ domains, which is in line with other similar reports[16,42–44], thus indicating that this could be a general mechanism. Moreover, structural studies demonstrate the predisposition of the PSD-95 tandem domains to engage in multivalent interactions; indeed, such a mode of interaction has been reported for MAGUKs in model systems[45,46]. These reports are consistent with the involvement of the three PDZ domains for the Stargazin–PSD-95 interaction observed in COS-7 cells. Together, these observations suggest that (i) multiple Stargazin binding motifs originating from an AMPAR complex can interact with the clustered PDZ domains of MAGUKs and (ii) the consequence of such an event is the stabilization of the overall supramolecular complex. In conclusion, because the divalent ligand, which is designed to reproduce this mode of binding, is necessary and sufficient to replicate the effect of PDZ domain–binding-deficient mutants of Stargazin, we have demonstrated that the stabilization of Stargazin-containing AMPARs at the synapse involves engaging in multivalent interactions with the PDZ domains of scaffold proteins.

The approach developed for the design of divalent AMPAR–Stargazin-competing ligands also provides us with probes that are specific for the targeted interaction. First, *in vitro* characterization of the divalent ligand on the basis of the 15-residue binding motif of Stargazin demonstrates a significantly enhanced affinity for

PSD-95–like tandem PDZ domains while showing weaker binding to other synaptic class I and II PDZ domains including PSD-95-3, Shank3 and GRIP. This behavior recapitulates the reported specificity of the native protein[4,35], further illustrating the biomimetic character of the ligands. Furthermore, experiments in cultured neurons using two different techniques demonstrate that specificity is not limited to the targeted PDZ domains but also extends to the interactions that are being disrupted by action of the ligands in the cellular environment. In particular, under conditions identical to those in which AMPAR properties are affected, the Stargazin-derived ligands elicit no observable effect on Shaker-type potassium channel mobility and NMDAR currents. It should be noted that although *in vitro* specificity, *in vivo* imaging (FRET-FLIM), receptor mobility and current measurements clearly support the target ligand specificity, it has not been feasible to exploit immunoprecipitation methods to demonstrate the specificity of the targeted interactions in crude brain lysates. In this case, we believe that lysate preparation methods, which use relatively harsh conditions including detergent such as Triton X-100 and deoxycholate, affect the higher-order molecular assembly of the Stargazin-containing AMPAR complex and PSD-95 that forms the foundation for the same high-affinity interactions that we are probing in the PSD. Together, these studies establish the basis for future efforts to understand the origin of the ligand specificities and mechanism of action as well as the mode of stabilization of each multimeric channel–receptor complex in live cells or intact tissues.

Finally, it is interesting to compare the differences in the effects obtained by acute disruption of the endogenous AMPAR–TARP–MAGUK interaction with the divalent ligands to the effects that resulted from the overexpression of Stargazin-ΔC[3]. The two approaches differ significantly and, in particular, produce their effects on very different timescales. The acute disruption of the PDZ domain–mediated stabilization of AMPARs by the biomimetic ligands resulted in a large, but only transient, increase in AMPAR mobility, then a significant increase in AMPAR endocytosis. This is consistent with a model in which, upon release from anchoring at the synapse, AMPARs diffuse away from the PSD into the extrasynaptic membrane, reach the endocytic zone next to synapses and enter the recycling pathway[39]. In agreement with the idea that they induce AMPARs to leave synapses, the competing ligands induced a decrease in both evoked and miniature AMPAR synaptic currents. Notably, this decrease was only partial, the amplitude of the mEPSCs being even less affected than that of evoked EPSCs. This is in clear contrast to what was observed with Stargazin-ΔC, which induced a full disappearance of evoked and spontaneous EPSCs[3,4]. Overall, these results suggest that a subpopulation of AMPARs (~40%), specifically activated by spontaneous glutamate release, relies on additional synaptic stabilization. A potential explanation for this effect is either that other unidentified binding partners that are not competed off by the divalent ligand or a higher order of multivalency (for instance, dimers versus tetramers of TARPs) is involved. Interactions mediated by the C termini of the AMPAR pore-forming subunits could participate to this additional stabilization. The elucidation of the precise effect would require detailed analysis of the AMPAR complex subpopulation composition.

In summary, inspired by the supramolecular arrangements of both the AMPAR–TARP complex and the synaptic MAGUKs, we have designed peptide-based divalent ligands that mimic the presence of multiple Stargazin C-terminal motifs. These ligands have enhanced affinity for the multiple PDZ domains of PSD-95 and can compete efficiently against the endogenous PDZ domain–mediated interactions involved in stabilizing the AMPARs at the PSD. Our results provide evidence for a model in which the TARP-containing AMPARs are stabilized at the synapse by engaging in multivalent interactions with the PDZ domains of synaptic MAGUKs. Moreover, the studies also reveal the presence of multiple populations that differ in their degree of stabilization. Therefore, the multivalent peptide-based ligands constitute efficient new tools for the study of clustered PDZ domains and could provide a starting point for promising therapeutic agents.

METHODS

X-ray crystallography. The PSD-95 self-binding tandem PDZ domains were recombinantly expressed, purified and crystallized by sitting-drop vapor diffusion. Data sets were collected on the NSLS beamline X6A at Brookhaven National Laboratory, and the structure was solved from diffraction data by molecular replacement. See **Supplementary Methods** and **Supplementary Table 3** for additional details.

Divalent ligand synthesis. The synthesis of the various series of mono- and divalent peptide-based ligands in each series is presented in detail in the **Supplementary Information**. In summary, for the 4-DMAP–containing divalent ligands, the last 10, 15 and 20 amino acids from the Stargazin PDZ domain–binding motifs were first assembled by standard SPPS with Fmoc-Dab(Alloc)-OH inserted at the −5 position. The peptides were next capped with a mixture of pentynoic acid and azidoacetic acid (3:4) before ligation by Cu(I)-catalyzed 1,3-dipolar cycloaddition[25] on resin. The 4-DMAP anhydride[47] was coupled to the ligand on-resin after Alloc deprotection[48]. Ligands used for cellular studies were synthesized by Fmoc-based SPPS up to position −14. Pentynoic acid was coupled using standard conditions as a 3:7 mixture with Fmoc-Dab(Alloc)-OH. The azidoacetic acid was then coupled to the Dab side chain amino group after addition of Boc-Cys(Trt)-OH and Alloc deprotection performed as previously reported[48]. The click chemistry ligation was performed as it was with 4-DMAP–containing divalent ligands. Cell-permeable ligands were obtained by reaction of the N-terminal cysteine residue with Ac-[$TAT_{47–57}$]-glycine-OSBn (native chemical ligation)[31,32]. The BODIPY FL dye was coupled using a maleimide derivative to the same cysteine residue. Peptide-based ligands were stored as lyophilized powder at −80 °C until use.

Fluorescence-based titrations. Fluorescence spectra were recorded in 1-cm path length quartz cells (100 or 450 µl nominal volume) at 25 °C. The spectra were corrected for emission intensity by using manufacturer-supplied correction factors. Slit widths were 3 nm and 6 nm for excitation and emission, respectively. The 4-DMAP fluorophore was excited at 421 nm, and the spectra were recorded between 432 nm and 730 nm (0.5 nm increments and 0.1 sec integration time). All titrations were conducted at least in triplicate.

FRET-FLIM measurements. FLIM was performed with the time-correlated single-photon counting (TCSPC) method on a multiphoton SP2 AOBS Leica confocal system using a HC Plan Apo CS ×63/1.32 NA objective. The pulsed light source was a tunable titanium-sapphire laser (Chameleon, Coherent). Two-photon excitation of EGFP was achieved at 900 nm. The laser repetition frequency was 80 MHz, which gave a 13-ns temporal window for lifetime measurements. The system was equipped with the TCSPC from Becker and Hickl (Germany) composed of a PMC-100 detector characterized by a transit-time spread of approximately 150 ps and a SPC 830 photon-counting and timing electronic card. A 510/40 nm band-pass filter was used to specifically detect the donor fluorescence. Fluorescence decay curves were obtained using single-spot mode of SPCM software (Becker and Hickl). The relative FRET efficiency was calculated for each acquisition as:

$$\text{FRET efficiency (\%)} = 100 \times (\tau_D - \tau_{DA})/\ \tau_D$$

where τ is the mean lifetime obtained from the exponential fit of the decay curve of the donor (EGFP) alone (τ_D) or of the donor in the presence of the acceptor (mCherry) (τ_{DA}). Results are expressed as a mean FRET efficiency. The chimeric construct EGFP::mCherry was used as a positive control.

Electrophysiology. Ionotropic glutamate receptor–mediated synaptic currents were recorded in whole-cell voltage clamp. The extracellular solution composition is provided in the **Supplementary Methods**. The GABA-A receptors were blocked with 50 µM picrotoxin. AMPAR or NMDAR currents were pharmacologically isolated with, respectively, 50 µM NMDAR antagonist D-AP5 or 20 µM AMPAR antagonist NBQX. For AMPAR mEPSC recordings, spontaneous action potentials were blocked with 1 mM tetrodotoxin. The bath temperature was kept at 33–35 °C. Patch clamp microelectrodes (4–6 megaohms (MΩ) resistance) were filled with intracellular solution (see **Supplementary Methods**). Peptide-based ligand stocks (1–2 mM) were dissolved in intracellular solution and stored at −70 °C. Recordings were performed with an EPC 10 double patch-clamp amplifier (HEKA). Data were sampled at 20 kHz and low-pass filtered at 2.9 kHz, using PatchMaster v2.0 software (HEKA). To record evoked EPSCs, whole-cell patch clamps were established on pairs of cells located within the same microscope field (~20–40 µm apart). To test for monosynaptic transmission, one cell was stimulated in current clamp mode by injecting a 1-ms current pulse, while the other was recorded in voltage clamp mode (−70 millivolts (mV) or +40 mV for AMPAR or NMDAR EPSCs, respectively). The current amplitude was adjusted to the minimum necessary to elicit a postsynaptic response, typically between 400–600 pA, then kept constant

throughout the experiment. Stimuli were delivered every 10–15 sec or every minute, respectively, for AMPAR or NMDAR EPSCs, and responses were recorded in individual sweeps. Neuron pairs for which the latency between the peak of the presynaptic action potential and the peak of the EPSCs was smaller than 4 ms were retained as monosynaptically coupled[49]. The pairs were rejected when the series resistance in both cells was above 30–40 MΩ. Data analysis was performed with custom software written in Matlab (http://www.mathworks.com/). Sweeps were averaged over 1 or 5 min (for AMPAR or NMDAR EPSCs, respectively), and synaptic currents were detected using a scaled template algorithm[50].

Other methods. Cloning, protein expression and purification, competitive titrations, DLS, affinity-based isolation experiments, neuronal culture, delivery of peptide-based ligands, surface AMPA receptor immunolabeling and endocytosis, and AMPA receptor tracking area are listed in **Supplementary Methods**.

Accession code. The atomic coordinates and structure factors of the first two PDZ domains of PSD-95 have been deposited in the Protein Data Bank (code 3GSL).

Received 2 August 2010; accepted 8 November 2010; published online 26 December 2010

References

1. Shepherd, J.D. & Huganir, R.L. The cell biology of synaptic plasticity: AMPA receptor trafficking. *Annu. Rev. Cell Dev. Biol.* **23**, 613–643 (2007).
2. Díaz, E. Regulation of AMPA receptors by transmembrane accessory proteins. *Eur. J. Neurosci.* **32**, 261–268 (2010).
3. Bats, C., Groc, L. & Choquet, D. The interaction between Stargazin and PSD-95 regulates AMPA receptor surface trafficking. *Neuron* **53**, 719–734 (2007).
4. Schnell, E. *et al.* Direct interactions between PSD-95 and stargazin control synaptic AMPA receptor number. *Proc. Natl. Acad. Sci. USA* **99**, 13902–13907 (2002).
5. Aarts, M. *et al.* Treatment of ischemic brain damage by perturbing NMDA receptor- PSD-95 protein interactions. *Science* **298**, 846–850 (2002).
6. Cui, H. *et al.* PDZ protein interactions underlying NMDA receptor-mediated excitotoxicity and neuroprotection by PSD-95 inhibitors. *J. Neurosci.* **27**, 9901–9915 (2007).
7. Bertaso, F. *et al.* PICK1 uncoupling from mGluR7a causes absence-like seizures. *Nat. Neurosci.* **11**, 940–948 (2008).
8. Mammen, M., Choi, S.-K. & Whitesides, G.M. Polyvalent interactions in biological systems: implications for design and use of multivalent ligands and inhibitors. *Angew. Chem. Int. Edn Engl.* **37**, 2754–2794 (1998).
9. Vandenberghe, W., Nicoll, R.A. & Bredt, D.S. Stargazin is an AMPA receptor auxiliary subunit. *Proc. Natl. Acad. Sci. USA* **102**, 485–490 (2005).
10. Bedoukian, M.A., Weeks, A.M. & Partin, K.M. Different domains of the AMPA receptor direct stargazin-mediated trafficking and stargazin-mediated modulation of kinetics. *J. Biol. Chem.* **281**, 23908–23921 (2006).
11. Shi, Y., Lu, W., Milstein, A.D. & Nicoll, R.A. The stoichiometry of AMPA receptors and TARPs varies by neuronal cell type. *Neuron* **62**, 633–640 (2009).
12. Kim, K.S., Yan, D. & Tomita, S. Assembly and stoichiometry of the AMPA receptor and transmembrane AMPA receptor regulatory protein complex. *J. Neurosci.* **30**, 1064–1072 (2010).
13. Kim, E. & Sheng, M. PDZ domain proteins of synapses. *Nat. Rev. Neurosci.* **5**, 771–781 (2004).
14. Songyang, Z. *et al.* Recognition of unique carboxyl-terminal motifs by distinct PDZ domains. *Science* **275**, 73–77 (1997).
15. Sheng, M. & Sala, C. PDZ domains and the organization of supramolecular complexes. *Annu. Rev. Neurosci.* **24**, 1–29 (2001).
16. Long, J.F. *et al.* Supramodular structure and synergistic target binding of the N-terminal tandem PDZ domains of PSD-95. *J. Mol. Biol.* **327**, 203–214 (2003).
17. Xu, W. *et al.* Molecular dissociation of the role of PSD-95 in regulating synaptic strength and LTD. *Neuron* **57**, 248–262 (2008).
18. Schlüter, O.M., Xu, W.F. & Malenka, R.C. Alternative N-terminal domains of PSD-95 and SAP97 govern activity-dependent regulation of synaptic AMPA receptor function. *Neuron* **51**, 99–111 (2006).
19. Garcia, E.P. *et al.* SAP90 binds and clusters kainate receptors causing incomplete desensitization. *Neuron* **21**, 727–739 (1998).
20. Piserchio, A. *et al.* The PDZ1 domain of SAP90. Characterization of structure and binding. *J. Biol. Chem.* **277**, 6967–6973 (2002).
21. Elkins, J.M. *et al.* Structure of PICK1 and other PDZ domains obtained with the help of self-binding C-terminal extensions. *Protein Sci.* **16**, 683–694 (2007).
22. Doyle, D.A. *et al.* Crystal structures of a complexed and peptide-free membrane protein-binding domain: molecular basis of peptide recognition by PDZ. *Cell* **85**, 1067–1076 (1996).
23. Morais Cabral, J.H.M. *et al.* Crystal structure of a PDZ domain. *Nature* **382**, 649–652 (1996).
24. Wang, W., Weng, J., Zhang, X., Liu, M. & Zhang, M. Creating conformational entropy by increasing interdomain mobility in ligand binding regulation: a revisit to N-terminal tandem PDZ domains of PSD-95. *J. Am. Chem. Soc.* **131**, 787–796 (2009).
25. Rostovtsev, V.V., Green, L.G., Fokin, V.V. & Sharpless, K.B. A stepwise Huisgen cycloaddition process: copper(I)-catalyzed regioselective "ligation" of azides and terminal alkynes. *Angew. Chem. Int. Edn Engl.* **41**, 2596–2599 (2002).
26. Dakoji, S., Tomita, S., Karimzadegan, S., Nicoll, R.A. & Bredt, D.S. Interaction of transmembrane AMPA receptor regulatory proteins with multiple membrane associated guanylate kinases. *Neuropharmacology* **45**, 849–856 (2003).
27. Sainlos, M., Iskenderian, W.S. & Imperiali, B. A general screening strategy for peptide-based fluorogenic ligands: probes for dynamic studies of PDZ domain-mediated interactions. *J. Am. Chem. Soc.* **131**, 6680–6682 (2009).
28. Eugenio Vazquez, M.E., Rothman, D.M. & Imperiali, B. A new environment-sensitive fluorescent amino acid for Fmoc-based solid phase peptide synthesis. *Org. Biomol. Chem.* **2**, 1965–1966 (2004).
29. Fawell, S. *et al.* Tat-mediated delivery of heterologous proteins into cells. *Proc. Natl. Acad. Sci. USA* **91**, 664–668 (1994).
30. Schwarze, S.R., Ho, A., Vocero-Akbani, A. & Dowdy, S.F. In vivo protein transduction: delivery of a biologically active protein into the mouse. *Science* **285**, 1569–1572 (1999).
31. Dawson, P.E., Muir, T., Clark-Lewis, I. & Kent, S. Synthesis of proteins by native chemical ligation. *Science* **266**, 776–779 (1994).
32. Hackeng, T.M., Griffin, J.H. & Dawson, P.E. Protein synthesis by native chemical ligation: expanded scope by using straightforward methodology. *Proc. Natl. Acad. Sci. USA* **96**, 10068–10073 (1999).
33. Dirr, H., Reinemer, P. & Huber, R. X-Ray crystal-structures of cytosolic glutathione S-transferases. Implications for protein architecture, substrate recognition and catalytic function. *Eur. J. Biochem.* **220**, 645–661 (1994).
34. Choi, J. *et al.* Phosphorylation of stargazin by protein kinase A regulates its interaction with PSD-95. *J. Biol. Chem.* **277**, 12359–12363 (2002).
35. Ives, J.H., Fung, S., Tiwari, P., Payne, H.L. & Thompson, C.L. Microtubule-associated protein light chain 2 is a stargazin-AMPA receptor complex-interacting protein in vivo. *J. Biol. Chem.* **279**, 31002–31009 (2004).
36. Elias, G.M., Elias, L.A., Apostolides, P.F., Kriegstein, A.R. & Nicoll, R.A. Differential trafficking of AMPA and NMDA receptors by SAP102 and PSD-95 underlies synapse development. *Proc. Natl. Acad. Sci. USA* **105**, 20953–20958 (2008).
37. Kim, E., Niethammer, M., Rothschild, A., Nung Jan, Y. & Sheng, M. Clustering of Shaker-type K^+ channels by interaction with a family of membrane-associated guanylate kinases. *Nature* **378**, 85–88 (1995).
38. Marks, D.R. & Fadool, D.A. Post-synaptic density perturbs insulin-induced Kv1.3 channel modulation via a clustering mechanism involving the SH3 domain. *J. Neurochem.* **103**, 1608–1627 (2007).
39. Petrini, E.M. *et al.* Endocytic trafficking and recycling maintain a pool of mobile surface AMPA receptors required for synaptic potentiation. *Neuron* **63**, 92–105 (2009).
40. Fourgeaud, L. *et al.* The metabotropic glutamate receptor mGluR5 is endocytosed by a clathrin-independent pathway. *J. Biol. Chem.* **278**, 12222–12230 (2003).
41. Heine, M. *et al.* Surface mobility of postsynaptic AMPARs tunes synaptic transmission. *Science* **320**, 201–205 (2008).
42. Paduch, M. *et al.* Bivalent peptides as models for multimeric targets of PDZ domains. *ChemBioChem* **8**, 443–452 (2007).
43. Klosi, E., Saro, D. & Spaller, M.R. Bivalent peptides as PDZ domain ligands. *Bioorg. Med. Chem. Lett.* **17**, 6147–6150 (2007).
44. Bach, A. *et al.* Design and synthesis of highly potent and plasma-stable dimeric inhibitors of the PSD-95-NMDA receptor interaction. *Angew. Chem. Int. Edn Engl.* **48**, 9685–9689 (2009).
45. Pegan, S. *et al.* NMR studies of interactions between C-terminal tail of Kir2.1 channel and PDZ1,2 domains of PSD95. *Biochemistry* **46**, 5315–5322 (2007).
46. Goult, B.T. *et al.* Small-angle X-ray scattering and NMR studies of the conformation of the PDZ region of SAP97 and its interactions with Kir2.1. *Biochemistry* **46**, 14117–14128 (2007).
47. Sainlos, M. & Imperiali, B. Synthesis of anhydride precursors of the environment-sensitive fluorophores 4-DMAP and 6-DMN. *Nat. Protoc.* **2**, 3219–3225 (2007).
48. Sainlos, M. & Imperiali, B. Tools for investigating peptide-protein interactions: peptide incorporation of environment-sensitive fluorophores via on-resin derivatization. *Nat. Protoc.* **2**, 3201–3209 (2007).
49. Medina, I., Leinekugel, X. & Ben-Ari, Y. Calcium-dependent inactivation of the monosynaptic NMDA EPSCs in rat hippocampal neurons in culture. *Eur. J. Neurosci.* **11**, 2422–2430 (1999).
50. Clements, J.D. & Bekkers, J.M. Detection of spontaneous synaptic events with an optimally scaled template. *Biophys. J.* **73**, 220–229 (1997).

Acknowledgments

This research was supported by the Human Frontiers Science Program (RGP0007/2006, M.S., D.C. and B.I.), the European Commission Marie Curie postdoctoral fellowship (PICK-CPP to M.S.), grants from the Agence Nationale pour la Recherche (ChemTraffic to M.S. and D.C) and the Conseil Regional d'Aquitaine. The microscopy was done in the Bordeaux Imaging Center of the Neurosciences Institute of the University of Bordeaux II. The help of P. Legros is acknowledged. We are grateful to the staff at the National Synchrotron Light Source beamline X6A for access via the General User program and especially to J. Jackonic for assistance in data collection and reduction.

Author contributions

B.I. and M.S. designed the biomimetic ligands and developed their synthesis and characterization *in vitro*; M.S. performed the experiments. Crystallization of the PDZ domains and structural analysis was performed by M.S., N.B.O. and M.S. collected the data and solved the structure. The affinity-based isolation experiments were performed by M.S., C.T. and L.B. performed the mobility experiments. C.T. performed the electrophysiology and endocytosis experiments. C.P. and K.T. performed the FRET experiments. C.B. performed the cloning for FRET and neuronal cultures. B.I. and D.C. equally provided project management. The manuscript was written by M.S., B.I. and D.C. with input from C.T., N.B.O. and C.P.

Competing financial interests

The authors declare no competing financial interests.

Additional information

Supplementary information is available online at http://www.nature.com/naturechemicalbiology/. Reprints and permissions information is available online at http://npg.nature.com/reprintsandpermissions/. Correspondence and requests for materials should be addressed to D.C. or B.I.